nature plants

ARTICLES

https://doi.org/10.1038/s41477-017-0064-y

Maintenance of carbohydrate transport in tall trees

Jessica A. Savage[1,2*], Sierra D. Beecher[3], Laura Clerx[2], Jessica T. Gersony[2], Jan Knoblauch[3], Juan M. Losada[2], Kaare H. Jensen[4], Michael Knoblauch[3] and N. Michele Holbrook[2]

Trees present a critical challenge to long-distance transport because as a tree grows in height and the transport pathway increases in length, the hydraulic resistance of the vascular tissue should increase. This has led many to question whether trees can rely on a passive transport mechanism to move carbohydrates from their leaves to their roots. Although species that actively load sugars into their phloem, such as vines and herbs, can increase the driving force for transport as they elongate, it is possible that many trees cannot generate high turgor pressures because they do not use transporters to load sugar into the phloem. Here, we examine how trees can maintain efficient carbohydrate transport as they grow taller by analysing sieve tube anatomy, including sieve plate geometry, using recently developed preparation and imaging techniques, and by measuring the turgor pressures in the leaves of a tall tree in situ. Across nine deciduous species, we find that hydraulic resistance in the phloem scales inversely with plant height because of a shift in sieve element structure along the length of individual trees. This scaling relationship seems robust across multiple species despite large differences in plate anatomy. The importance of this scaling becomes clear when phloem transport is modelled using turgor pressures measured in the leaves of a mature red oak tree. These pressures are of sufficient magnitude to drive phloem transport only in concert with structural changes in the phloem that reduce transport resistance. As a result, the key to the long-standing mystery of how trees maintain phloem transport as they increase in size lies in the structure of the phloem and its ability to change hydraulic properties with plant height.

Trees dominate many terrestrial landscapes and can exceed 100 m in height. Yet, the question of how trees transport carbohydrates from the canopy where sugars are produced to their roots remains unanswered[1,2]. Carbohydrate transport occurs in the phloem and is thought to be driven by osmotically generated pressure differentials between sugar-rich regions, where carbon is fixed or stored, and sugar-poor regions, where carbon is used to fuel growth and metabolism[3]. This mechanism runs into problems when the distance between the canopy and the roots becomes large because the pressures predicted to drive transport become exceedingly high, reaching levels at which concomitant increases in viscosity should impede flow[4–6]. Herbaceous plants avoid this issue because they lack the transport distances that occur in trees and they also have the ability to increase phloem pressure in their source tissue[7] by using membrane transporters to load sugars against a concentration gradient[8]. However, in many of the trees examined so far, evidence suggests that carbohydrates enter sieve tubes by diffusion through plasmodesmata[9], precluding the development of sugar concentrations that exceed those of surrounding cells. As a result, trees should have lower phloem pressures than herbaceous plants[10]. If some trees lack the ability to increase phloem turgor pressure as they increase in size, how are they able to transport sugars from their leaves to their roots? The key to this dilemma might lie in the structure of the phloem.

Efficient vascular transport relies on the scaling of conduits in relation to organismal size to minimize the accumulation of hydraulic resistance, and hence energetic cost, with increasing transport length[11–13]. Studies of xylem structure, the part of the vascular system that transports water and nutrients from the soil to the leaves, show good agreement with such predictions because plants produce wider xylem conduits as they increase in size[14–17]. However, there are reasons to question whether the phloem can exhibit the structural variation needed to mitigate the build-up of phloem resistance with height. A major difference between xylem and phloem conduits is that the cells that make up xylem conduits, vessel elements, retain only their cell wall at maturity and have no cytoplasm. By contrast, the cells that form conduits in the phloem, sieve elements, have an intact plasma membrane with modified intracellular contents (for example, they have no nucleus or ribosomes), forcing them to rely on neighbouring companion cells for metabolic processes, including protein synthesis[18,19]. As a result, the maximum size of phloem conduits could be constrained by the ratio of cell volume to exchange surface area with companion cells, thus limiting the ability to produce wider phloem conduits as trees grow taller.

A second reason why the phloem may face structural constraints that do not occur in the xylem arises from differences in the connections between cells that make up the conduits: perforation plates in the case of the xylem, and sieve plates in the phloem. Because the phloem is under positive pressure, damaged areas must be isolated to prevent bleeding, which is often accomplished by rapidly occluding sieve pores with the polysaccharide callose[20]. As a result, a trade-off between sieve plate pore size and sealing efficacy could constrain the ability to produce sieve tubes with lower hydraulic resistance. A similar constraint does not occur in the xylem because the homologous structures are not involved in a wound response, therefore allowing perforation plates to be completely open (that is, simple) in many species.

Because of these theoretical arguments and the lack of data available on phloem anatomy, most models of phloem transport assume that sieve tube structure is invariant within an individual tree[4,21,22].

[1]Department of Biology, University of Minnesota, Duluth, MN, USA. [2]Department of Organismic and Evolutionary Biology, Harvard University, Cambridge, MA, USA. [3]School of Biological Sciences, Washington State University, Pullman, WA, USA. [4]Department of Physics, Technical University of Denmark, Lyngby, Denmark. *e-mail: jsavage@d.umn.edu

In a notable exception, Hölttä et al. showed that modelled transport rates are more in line with expected values if sieve tube resistance decreases with plant height[23]. However, relatively few studies have investigated how sieve tube diameter changes along the length of a tree[24–27]. Moreover, even if widening occurs, sieve plate resistance, which often contributes >50% of the resistance in the system, could still limit phloem transport[28,29].

Despite more than a century of research on phloem transport[30], one of the biggest obstacles in studying phloem transport is accurately measuring all of the components involved in driving transport in the tissue[7]. The situation is further complicated when studying the long path lengths found in trees[4,23,31]. However, with the introduction of new methods for investigating the structure of the phloem[28,32] and measuring phloem pressure[7,33], it is possible to test whether phloem anatomy and loading limit carbon transport in tall trees. In this study, we apply these new methods to investigate the structure of phloem and xylem conduits at multiple heights along the main axes of nine angiosperm tree species, and relate the driving force for phloem transport with estimates of phloem hydraulic resistance in a 25-m-tall red oak tree (*Quercus rubra*). With these experiments, we seek to reveal the factors that enable long-distance carbohydrate transport to the roots of tall trees, and demonstrate that a passive transport mechanism is feasible in the phloem if we change core assumptions in our understanding of the developmental biology of sieve elements and in our transport models about phloem resistance.

Results

Phloem structure and resistance scale inversely with plant height. To elucidate phloem hydraulic architecture, we collected anatomical data on parameters that influence flow characteristics in transport cells (Fig. 1). By mapping changes in cell structure from distal branches to the base of the stem, our data reveal striking variation in key parameters, including sieve element radius, r, sieve element length, l, and sieve pore radius, r_p (Fig. 2a–d). All three of these parameters are positively correlated with distance to the top of the tree across species (logistic regression (LR): $\alpha = 0.001$; see Supplementary Information 1, Supplementary Table 1) and are significantly larger at the base than at the top of each tree (paired t-test: $\alpha = 0.001$; see Supplementary Information 1, Supplementary Table 2). The fourth parameter we measured, sieve pore number, N, did not correlate with height across species (LR: $F_{1,28} = 1.89$, $P = 0.18$).

We examined the effect of variation in anatomical parameters (Fig. 1) on carbon transport by estimating the phloem hydraulic resistance, R, in an individual sieve tube. This can be expressed as $R_{tube} = R_{lumen} + R_{plate}$ where the lumen resistance is

$$R_{lumen} = \frac{8\eta l}{\pi r^4} \quad (1)$$

Plate resistance is calculated as the sum of the resistances of all the pores, which we estimated based on the average pore size and the number of pores per plate[28]. For this calculation, we assume laminar flow and that the pores have a normal distribution. We also assume a sap viscosity of $\eta = 1.7$ MPa s, which is an estimate consistent with recent pressure measurements in situ, data collected from sap sugar concentrations and models of optimal viscosity[7,34]. Across all nine species (ten trees) in the study, we find that sieve tube resistance per unit length (R_{tube}/l) scales inversely with the distance from the top of the tree (LR: $F_{1,28} = 127$, $P < 0.0001$; Fig. 2a). We looked at this relationship in terms of distance from the top of the tree because it provides an estimate of the maximum distance from the source leaves.

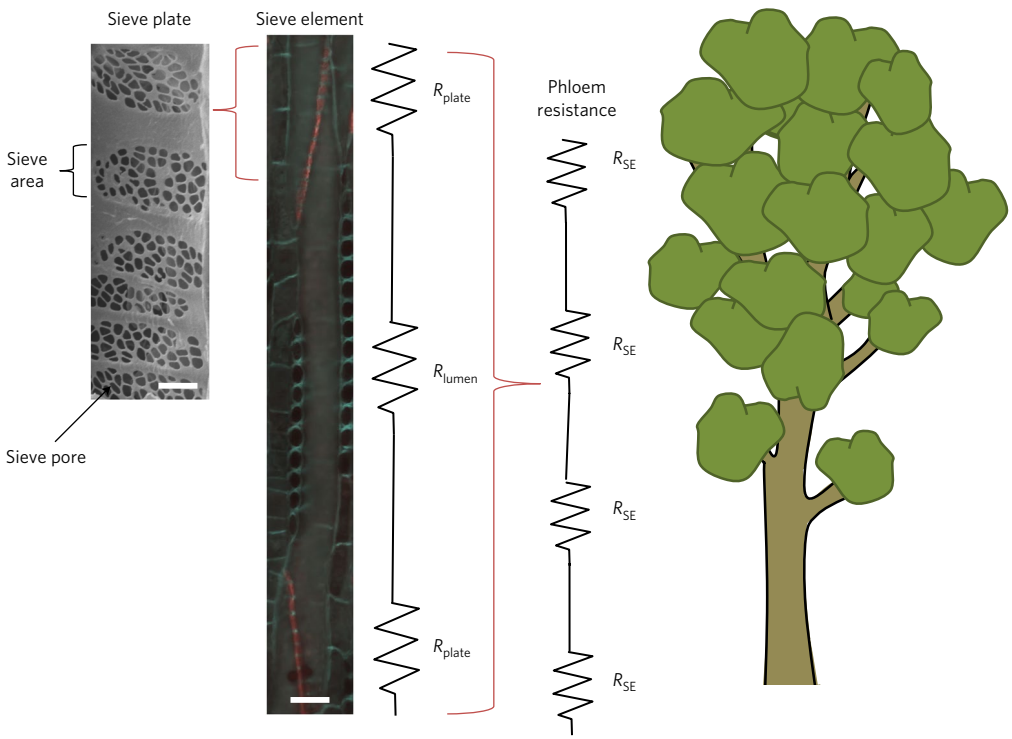

Fig. 1 | Diagram of sieve tube anatomy and structural parameters that contribute to hydraulic resistance in angiosperms. Sieve tubes are conduits that are composed of individual cells, separated by plates with pores. R_{lumen} and R_{plate} are additive along the length of a tree, leading to a higher predicted resistance in taller trees. The resistance at different points along the tree can be calculated based on a series of anatomical parameters. Scale bars in the sieve plate and sieve element (SE) micrographs are 10 μm and 20 μm, respectively.

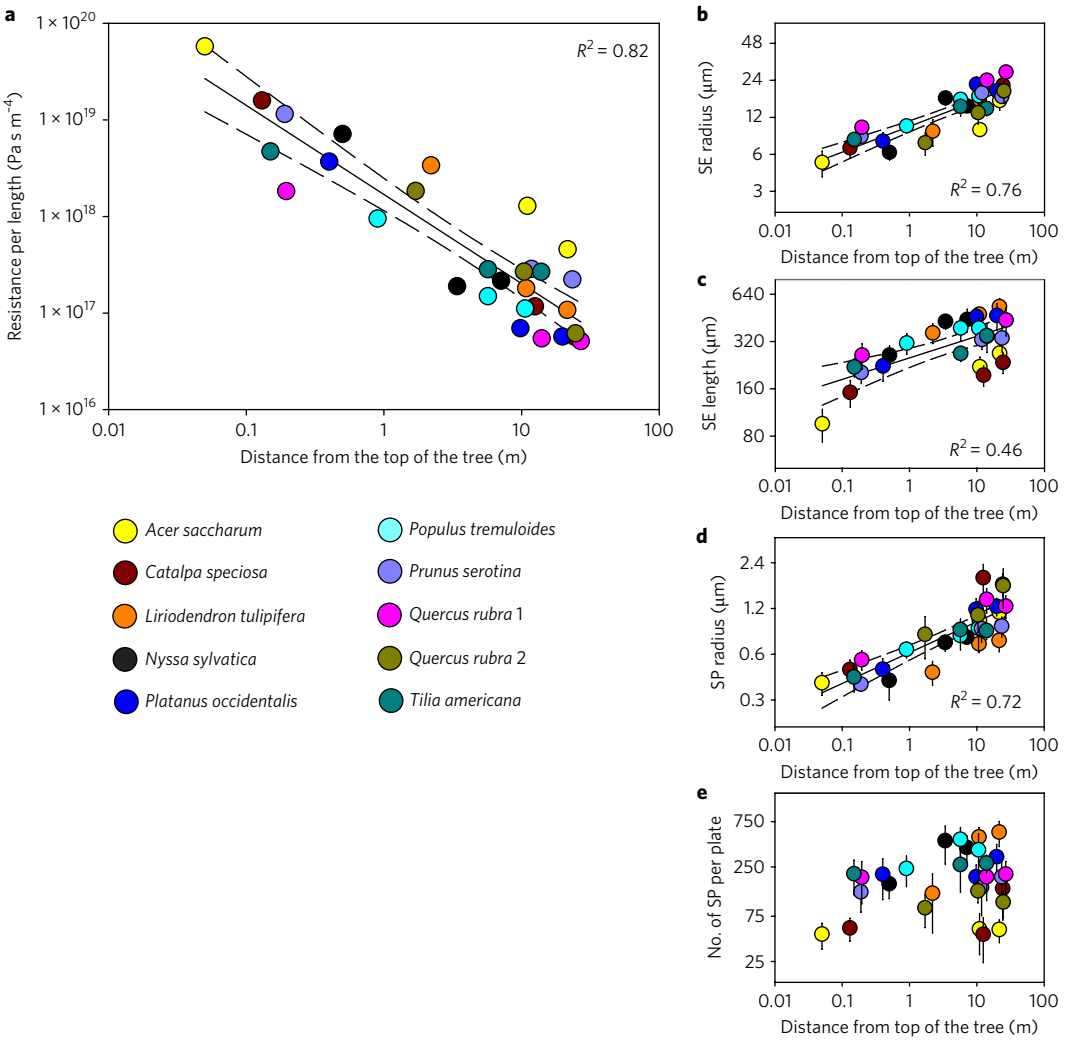

Fig. 2 | Relationship between phloem anatomical parameters and height. a–e, Regression of resistance per unit length (**a**), sieve element (SE) radius (**b**), sieve element length (**c**), sieve pore (SP) radius (**d**) and the number of sieve pores per plate (**e**) on height of the tissue sample. The sample height gives us an indication of the maximum distance to the source leaves. The graphs include data from three height levels of ten plants, with the exception of sieve element length, which was only measured on nine plants. The solid black lines are best-fit linear regression with a 95% confidence interval (dashed lines) for all significant relationships ($\alpha = 0.001$). Error bars are ±1 s.d.

Phloem scaling reduces the pressure required for carbon transport. To illustrate the consequences of this inverse scaling, we consider the pressure needed to drive phloem sap along a single continuous sieve tube, that is, the length of a tall tree from the top of the canopy to the roots. We modelled the pressure, Δp (in Pa), required to drive sap flow rate, Q (in m^3 s^{-1}), using a resistor analogy

$$\Delta p = QR \tag{2}$$

where R is measured in Pa s m^{-3}.

We then calculated the pressure required to drive transport assuming that phloem structure was uniform throughout a tree. For this calculation, we held resistance per unit length and sieve tube radius at the average values recorded at the top of the trees (small branches): 1×10^{19} Pa s m^{-4} and 7 µm, respectively. We assumed that the phloem had a constant viscosity and a constant flow speed along the entire plant. We selected a flow speed of $u = 156$ µm s^{-1} based on the average measurement in angiosperms[35–39]. This value is of a similar order of magnitude to the speed (180 µm s^{-1}) measured in a different oak species, *Quercus robur*, using ^{11}C positron emission tomography imaging[36]. Using these parameters, we find that a pressure of

$$\Delta p \simeq \frac{\pi r^2 u L R_{\mathrm{tube}}}{l} = 6\,\mathrm{MPa} \tag{3}$$

is required to drive flow in a tall tree that is $L = 25$ m. However, the sugar concentration necessary to generate a phloem pressure of 6 MPa would inhibit transport because of its viscosity[34].

If we modify our model to take into account the variation in phloem structure that we observed along the stem of this tree and compute the pressure required to drive flow by summing the contribution from the conduits in series, this leads to

$$\Delta p = Q \sum_{i}^{n} R_{\mathrm{tube},i} \simeq \int_{l_0}^{L} \frac{R_{\mathrm{tube}}}{l} dx \tag{4}$$

where the sum is taken over all the conduits in series, and the integral is between the top (at $x = l_0 = 0.1$ m) and the base of the

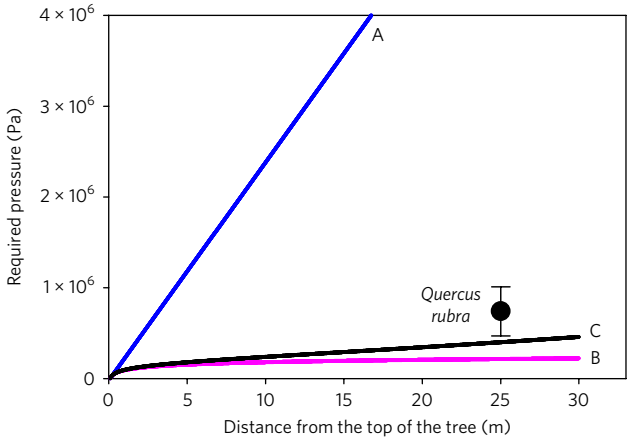

Fig. 3 | Model of pressure differential required to drive phloem transport with increasing tree height under three different scenarios. In scenario A, sieve tube structure is uniform along the length of the tree, and in scenarios B and C, sieve tube structure scales with height as observed in Fig. 2a. Scenarios B and C are different in their assumptions about the cross-sectional area of the phloem; in scenario B, the cross-sectional area of the phloem increases with conduit size, and in scenario C, it is held constant along the length of the tree. All three models assume a flow rate of 156 µm s^{-1} and a sap viscosity of 1.7 MPa s. The pressure data from the red oak tree at $L = 25$ m is also shown (black dot). Error bar is ±1 s.d. ($n = 6$).

plant (at $x = L = 25$ m). In our data, R_{tube}/l scales inversely with maximum distance x from the source leaves as $R_{tube}/l = A/x$, where $A = 1.6 \times 10^{18}$ Pa s m^{-4}. This yields a pressure differential of

$$\Delta p = Q \int_{l_0}^{L} \frac{A}{x} \mathrm{d}x = QA \log\left(\frac{L}{l_0}\right) = 0.2\ \mathrm{MPa} \quad (5)$$

Thus, the variation in phloem structure observed reduces the pressure required to drive flow by more than a factor 10 compared with the invariant case (Fig. 3, scenario A versus scenario B). To extrapolate the structural adjustments to even taller trees, we compared the ratio of pressures required to drive the same flow rate, Q, in two trees of length, L_1 and L_2,

$$\frac{\Delta p_1}{\Delta p_2} = \frac{\log\left(\frac{L_1}{l_0}\right)}{\log\left(\frac{L_2}{l_0}\right)} \quad (6)$$

Remarkably, considering projected variation in phloem anatomy of a tall tree that is $L_1 = 100$ m, the pressure is only 1.5-times greater than what is needed to drive flow in a tree that is $L_2 = 10$ m. Without the observed scaling of sieve tube structure along the stem, a tenfold increase in pressure would be needed.

In the previous analyses, flow rate was assumed constant, whereas the conduit radius (and sieve plate properties) changed along the translocation axis. This implies that the conductive area at the base is larger than at the top. An alternative scenario is to fix the total conductive area (Supplementary Information 2). Under this scenario, the pressure required to drive transport in a 25-m tree is 0.4 MPa. Although slightly higher than scenario B, both of these scenarios (B and C) predict pressures that are much smaller than what is predicted from uniform conduits, $\Delta p_A = 6$ MPa (Fig. 3).

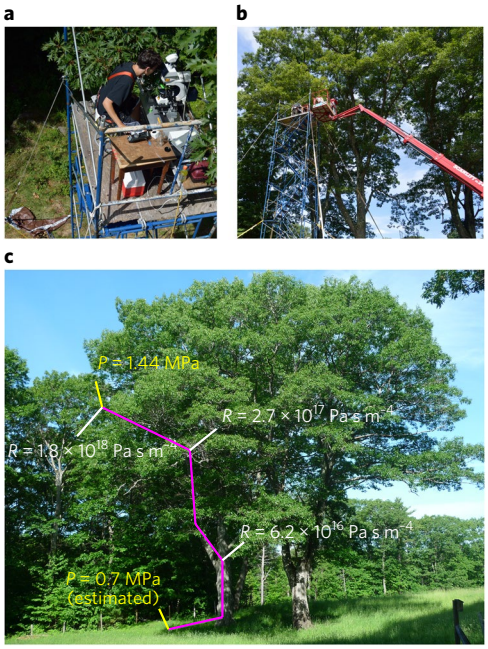

Fig. 4 | Parameterization of carbohydrate transport in a 120-year-old red oak tree. a,**b**, A fixed-stage fluorescence microscope system with a digital camera, micromanipulator and a vibration insulation system is placed on a 12 m scaffolding to access source leaves on a red oak tree for in situ turgor pressure measurements. **c**, Changes in resistance per unit length and pressure along the length of the tree. Based on the high conductivity, the turgor pressure of 1.44 MPa (±0.27 MPa s.d.; $n = 6$) in source mesophyll cells is sufficient to drive flow over a distance of 25 m from the canopy to the root tips.

Trees generate sufficient turgor pressure to drive flow from leaves to roots. We next tested whether there is sufficient pressure in the leaves to drive phloem transport to the roots of a 25-m-tall red oak tree. Pressure measurements of individual cells are exceedingly difficult to make even in the laboratory[33] and had never been attempted in a tree canopy prior to this study. To do this, we assembled a portable fluorescence microscope with active vibration insulation, micromanipulators and movie cameras (Fig. 4a,b) on scaffolding adjacent to the tree that was 12 m high. We measured the leaves on a branch with a distance to root sinks of 25 m (Fig. 4c) during the day when stomata were open and leaf water potentials were near their minimum (−1.1 MPa (±0.47 s.d.)).

We assume that *Q. rubra* is a passive-loading species based on previous research[9]. Under this scenario, the highest turgor pressure that drives photoassimilate transport should exist in the mesophyll cells. Thus, we inserted pico gauges through the epidermis for pressure measurements in mesophyll cells and recorded an average source turgor of 1.44 MPa (±0.27 s.d.). Despite our assumption about loading type, we acknowledge that there is evidence that not all oak species are passive loaders[40,41]. However, we expect this will have limited impact on our analysis because an active-loading species should have higher source pressure.

Based on previous work, the pressure in root cortical cells is within the range of 0.4–0.7 MPa[7,42–44]. If we assume that the sink turgor is similar among species and conservatively select the highest value in this range to put into our model (0.7 MPa), we estimate that the minimum pressure difference from source to sink in our oak tree is about 0.74 MPa. This is greater than the 0.2 MPa that is required to drive phloem transport based on the model described above. Thus, these data indicate that there is sufficient pressure to

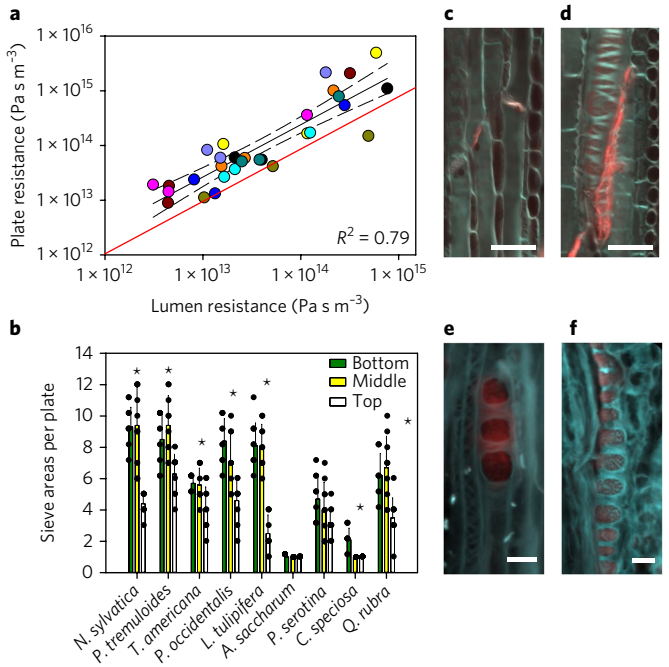

Fig. 5 | Structural changes in sieve plate anatomy that affect sieve tube resistance. a, The correlation between sieve plate resistance and lumen resistance in an individual sieve element. The graph includes data from three height levels of ten plants. The solid black line is a best-fit LR ($P < 0.0001$) with a 95% confidence interval, the 1:1 line is red and symbol/colour combinations indicate the plant (see Fig. 2 for key). Dashed lines indicate the 95% confidence interval. **b**, Variation in the number of sieve areas at different locations along the stem for all the species in the study. Significant differences ($\alpha = 0.001$) within species are noted with an asterisk and the colours of the bars indicate sampling location. The black circles show the raw data of sieve area number. Species are ordered from tallest to shortest. Error bars are ±1 s.d. ($n = 10$ per sample). **c–f**, Confocal micrographs of sieve tubes and sieve plates from longitudinal sections of a branch and the trunk of *P. tremuloides* (**c**,**d**) and *N. sylvatica* (**e**,**f**). Callose on the sieve plates is stained with aniline blue (magenta). Scale bars are 40 µm (**c**), 50 µm (**d**), 10 µm (**e**) and 20 µm (**f**).

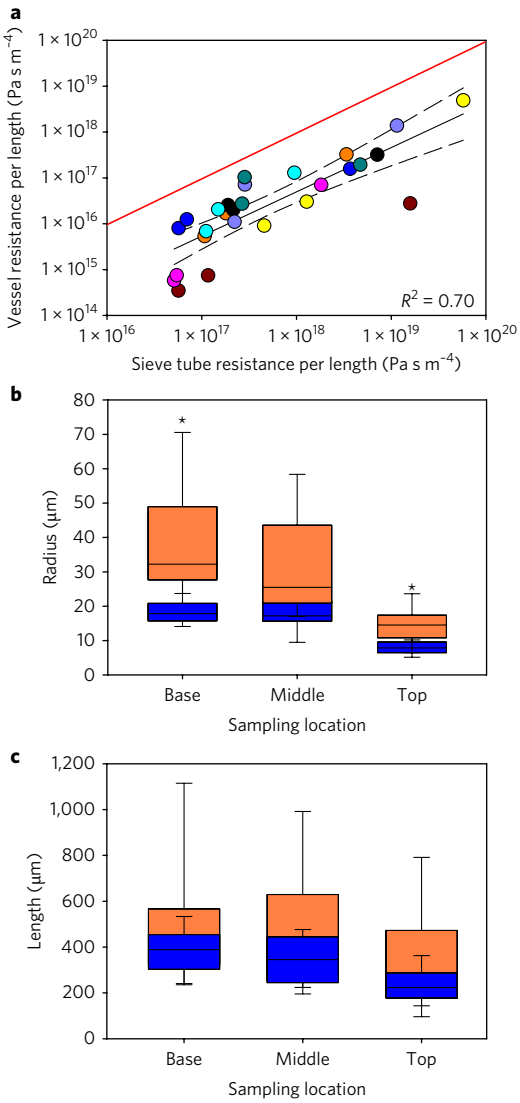

Fig. 6 | Comparison of xylem and phloem anatomy. a, Correlation between sieve tube resistance and vessel resistance on a length basis in nine tree species. Each plant was sampled at three heights. The solid black line is best-fit LR ($P < 0.0001$) with a 95% confidence interval (dashed lines), the 1:1 line is red and the symbol/colour combinations indicate the plant (see Fig. 2 for key). **b**,**c**, Boxplot of conduit radius (**b**) and length (**c**) in vessel elements (orange) and sieve elements (blue) along the length of a tree. The centre is the median and the range is noted with bars. Significant differences between the sieve element and the vessel element based on a two-sided, paired *t*-test are noted with an asterisk ($\alpha = 0.01$). Sample numbers are given in Methods.

drive carbohydrate transport from the canopy to the roots because of anatomical changes in phloem structure despite the water potential gradient in the xylem.

Scaling of phloem resistance arises from changes in both R_{lumen} and R_{plate}. Across species, there is a strong correlation between lumen and plate resistance in sieve tubes (LR: $F_{1,28} = 105$, $P < 0.0001$; Fig. 5a), and both aspects of resistance scale with height (see Supplementary Information 1, Supplementary Fig. 1). Although changes in lumen resistance are driven by conduit radius, plate resistance can be attributed to several factors including pore number and pore size depending on the plate structure of the species (Fig. 5b–f). For example, seven species with multiple sieve areas (that is, compound plates) increase the number of sieve areas on their plates and, therefore, their pore number near the base of their stem (Fig. 5b and see Supplementary Information 1, Supplementary Table 3). *Prunus serotina* was the only species with compound plates where this change was not significant (Kruskal–Wallis: $\chi^2 = 4.93$, $P = 0.08$). By comparison, *Acer saccharum*, which has simple plates, showed no change in pore number along its length (Fig. 5b).

Overall, there is no evidence that compound and simple plates are inherently different in their resistance despite large differences in pore number, which is consistent with a previous study[29]. Instead, we find that the number of sieve areas only correlates with the sieve element length and plate angle (see Supplementary Information 1, Supplementary Fig. 2, Supplementary Table 4). This is because changes in pore number and pore size are not equivalent in terms of their effect on plate resistance: increasing the number of pores per plate only has a modest effect on plate resistance. If we assume nothing else changes in plate structure, adding 130 pores (the average increase from the top to the bottom of the stem for species in this study) would decrease plate resistance by twofold. Note that, when adding this number of pores, the covering fraction of the plates does not exceed 67% (±4% s.d.). By contrast, sieve pore size is highly influential because resistance scales

inversely with pore radius to the third or fourth power. This is probably why pore radius correlates with plant height across all species (LR: $F_{1,28}=90.3$, $P<0.0001$; Fig. 2d).

Xylem and phloem conduits exhibit similar scaling with plant height. Xylem and phloem conduits develop from the same pluripotent cambial initial cells, and scaling models predict that both the xylem and the phloem should exhibit similar patterns in relation to transport length. However, the fact that phloem conduits remain living has long been thought to constrain the size and, therefore, the hydraulic properties of sieve tubes. Our data show that the hydraulic resistance of the xylem and the phloem scales similarly with height (LR: $F_{1,25}=59.1$, $P<0.0001$; Fig. 6a). One driver of this pattern is changes in conduit radius; both sieve tube and vessel radius scale with plant height (see Supplementary Information 1, Supplementary Fig. 3), and the scaling exponent for these two curves is not significantly different (that is, there is no significant tissue × distance interaction: $F_1=0.13$, $P=0.07$). There is also a correlation between element length in both tissues (LR: $F_{1,25}=43.2$, $P<0.0001$) and the longest elements that occur at the base of the tallest trees.

Despite similarity in the scaling between the xylem and the phloem, resistance per length in the phloem is on average an order of magnitude greater than in the xylem (Fig. 6a). This is partly because sieve tubes are two-to-six-times narrower than vessels (Fig. 6b and see Supplementary Information 1, Supplementary Table 5). Transport in the xylem is also less impeded by cell–cell boundaries because perforation plates in the xylem of most of the species in this study are completely open. However, in the phloem, the total pore area of a plate never exceeds the cross-sectional area of a sieve plate, that is, the covering fraction is always <1 (average: 0.3 (±0.1 s.d.). Additionally, sieve tube elements are often shorter than vessel elements (Fig. 6c), with the greatest difference in our study (>500 µm) occurring in *Nyssa sylvatica*. This means that the phloem has a higher frequency of plates along its pathway. In the xylem, the main source of resistance besides the lumen is the endwalls of the vessels. There is no analogous structure in the phloem because sieve tubes are thought to extend the entire length of a plant. In this study, we assumed that, based on previous work[45], vessel endwalls and the vessel lumen contribute equally to vessel resistance on a length basis.

Discussion

The feasibility of Münch pressure flow in tall trees has often been called into question because of the perceived challenges that are associated with transporting sugars across long distances in the phloem[4,5,31,46]. Indeed, the difficulty in accommodating passive transport in large plants with low phloem pressures provided strong impetus for the development of alternative hypotheses for phloem transport[30], including electro-osmosis across sieve plates[47,48] and serial zones of loading and re-loading[49,50]. Here, we show that because of modification of sieve tube size and sieve plate structure along the stem, the pressure required to drive carbohydrate transport from the top of the canopy to the roots of tall trees is essentially independent of organism size (Fig. 2). The striking changes observed in sieve tube anatomy in this study obviate the need for scaling of phloem pressure with height, which explains how plants that load symplastically can rely on Münch pressure flow for carbon transport (Fig. 3). We also show that, consistent with synthetic models of passive phloem loading[51], the pressures measured in the leaves of a mature oak tree are large enough to support transport to the roots even if we conservatively assume a passive-loading mechanism (Fig. 4). Considering that passive loading avoids the energy expenditure that is needed to concentrate sugars in sieve tubes, it is now clear why there would be no selective pressure for trees to deviate from the ancestral passive-loading mechanism[52,53] purely based on vertical stature.

It has long been known that xylem conduits widen near the base of trees, but limited research on variation in sieve tube anatomy within individual plants exist owing to the assumption that phloem structure is invariant (except see refs [24–27]). Our data clearly show that sieve tubes demonstrate a similar widening as vessels and that resistance in the two vascular tissues is strongly correlated despite differences in the absolute radius, the length of the conduit elements and the resistance of their plates (Fig. 6). This demonstrates that the similar scaling of the two vascular tissues is not solely the result of their shared origin from cambial initials, but instead reflects structural requirements for efficient vascular transport[11,13], a conclusion that is further supported by a recent study of the scaling of xylem and phloem conduits in *Populus* leaves[54]. The fact that we see widening as opposed to uniformly wide tubes suggests that there is a cost to larger tubes. This has been widely observed in other circulatory systems, including in the xylem[11–13,15,54].

One of the remarkable features of this study is that the scaling of sieve tube resistance is shared across all species, despite their anatomical differences. This is especially true in the case of sieve plate resistance, which varies by species in terms of the aspects of plate structure that change along their stem (for example, pore radius and pore number). With *A. saccharum*, which has simple sieve plates, scaling of plate resistance is driven solely by changes in pore size, whereas in *Q. rubra*, which has compound plates, there is an increase in pore size and pore number (Fig. 5). Our study documents consistent changes in sieve plate anatomy along the length of individual trees; this pattern is critical in reducing a length penalty on phloem transport because plates constitute >50% of the total transport resistance in the tissue. Our results also show how the relationship between plate anatomy and plant height across species[29] is driven by changes that occur within individual plants as they grow taller.

The demands of moving water through the xylem have often been posed as setting limits to tree height[55–57]. Similar constraints have been proposed for carbohydrate movement[23,58], but the data needed to evaluate this hypothesis have been lacking. Here, we show that pressures in leaves are sufficient to drive phloem transport only in combination with a marked reduction in sieve tube resistance along the length of the stem of a mature red oak tree. Without these adjustments, this tree would need pressures that are tenfold larger, which are greater than those measured in this study (and larger than those measured in active-loading plants[7]). As a result, the structure of the phloem is the key in solving the long-standing question about the feasibility of long-distance carbohydrate transport. However, with this discovery comes new questions about how scaling of sieve tube structure along the stem axis is controlled. Although there is some research examining the role of both auxin and water potential in determining conduit radius in the xylem[59,60], we know relatively little about how sieve element structure is regulated during development. Future research in this area could help us to understand how different species are able to achieve a similar scaling with height, despite anatomical differences in sieve plate structure, and therefore improve our understanding of the role of phloem structure in plant growth and productivity[61,62].

Methods

Sample collection. Xylem and phloem samples were collected from ten trees at three heights: one at the base of the stem, one halfway up the stem and one on a distal branch near the top of the tree (Table 1). Pieces of each sample were divided into sections that were frozen in liquid nitrogen, preserved in 70% ethanol or processed while fresh depending on the requirements for the subsequent analysis. We also measured the height and the diameter of the stem at each sample location and the total plant height. Plant material was collected from the Arnold Arboretum (Boston, MA, USA), Harvard Forest (Petersham, MA, USA) and Harvard University Campus (Cambridge, MA, USA) (Table 1). Note that, with the red oak used for the pressure measurements (*Q. rubra* 2), we completed a more comprehensive sampling of the phloem and did not sample the xylem.

Sieve tube anatomy. Samples preserved in ethanol were sectioned radially by hand and stained with a mixture of 0.1% aniline blue and 0.1% calcofluor white in 10 mM CHES buffer with 100 mM KCL (pH 10). We imaged the sections using either a LSM 510 confocal with a 405 nm laser (Zeiss) or a DMI 3000 inverted fluorescent microscope using an A4 filter (Leica). We measured sieve element

Table 1 | Trees included in the study

Plant	Height (m)	Collection site[a]
Acer saccharum Marsh.	21.7	Harvard Forest
Catalpa speciosa Warder ex Engelm.	24.5	Arnold Arboretum, non-accessioned
Liriodendron tulipifera L.	21.6	Harvard Forest
Nyssa sylvatica Marshall	7.2	Harvard Campus
Platanus occidentalis L.	20.0	Arnold Arboretum, 1236-79*D
Populus tremuloides Michx.	10.7	Harvard Campus
Prunus serotina Ehrh.	23.5	Harvard Forest
Quercus rubra L. 1	27.0	Harvard Forest
Quercus rubra L. 2	25.0	Harvard Forest
Tilia americana L.	14.0	Arnold Arboretum, 17527*D

[a]Accession numbers are given for samples collected at the Arnold Arboretum.

length and lumen radius in ten cells per sample with the exception of *Q. rubra* 2, which was used for the pressure measurements. In this plant, we measured lumen radius in 20 cells and estimated the length to be 350 µm, a value that is comparable to the other red oak tree in the study. Because sampling protocols are not standardized for measuring phloem anatomy, we determined the sample replication required to produce a similar coefficient of variation to our xylem analysis for which sampling was determined based on established standards[63].

Frozen samples were thawed and sectioned at a similar angle to sieve plates (for example, transversely for samples with plates that were perpendicular to tube walls, and longitudinally for samples with angled plates). The material was incubated for a minimum of 2 weeks at 54 °C in a mixture of 0.1% proteinase K dissolved in 50 mM Tris-HCL buffer, 1.5 mM Ca^{2+} acetate and 8% Triton X-100 (pH 8.0)[32]. After rinsing, they were freeze dried for 24 h and mounted on scanning electron microscopy (SEM) stubs. Samples were sputter coated with 10 nm gold using an EMS 300 T D Dual Head Sputter Coater (Electron Microscopy Sciences) at the Harvard Center for Nanoscale Systems, and imaged using a JEOL-6010LV SEM microscope (JEOL) at the Arnold Arboretum under high vacuum using an accelerating voltage of 10 kV. We estimated the size of every visible pore on 6–15 plates (100–1,500 pores per sample) and estimated the total number of pores on 10 plates per sample according to a previous study[32]. Supplementary Information 1, Supplementary Table 6 lists the number of pores measured for each of the 30 samples. For compound plates, the average number of pores per plate was calculated based on the number of pores per sieve area (estimated from ten SEM images) and the number of sieve areas per plate (estimated from ten cells imaged with a confocal microscope).

Vessel element anatomy. Cross-sections were made of fresh samples using a sliding microtome. They were stained with 0.05% toluidine blue in PO_4 buffer (pH 5.5) and imaged on a Leica DMI 3000. We measured the lumen area of vessels in 25% of the outer growth ring (100–740 vessels per sample). Supplementary Information 1, Supplementary Table 6 lists the number of vessels measured for each of the 27 samples. The remaining xylem tissue was macerated using a mixture of acetic acid and hydrogen peroxide[64]. The samples were incubated for 3–6 d at 56 °C and stained with 1% safranin O in 95% ethanol. Macerations were imaged on a Leica DMI 3000, and the length of 20 vessel elements was measured.

Source mesophyll turgor measurements in a red oak tree. We measured source mesophyll turgor in situ in a mature red oak tree, *Q. rubra* 2 (approximately 120 years old), in a group of three trees on pasture land that were well exposed to the sun located at 42° 31′ 59.47″ N, 72°11′29.34″ W at Harvard Forest. This tree was selected because of it long axis of sourceless stem and branches, its growth pattern of overhanging branches that are reachable with scaffolding and the possibility to take phloem samples at various locations.

A scaffolding of 12 m in height was assembled to reach a major branch with source leaves at a distance of 20 m from the stem base. A Leica fixed-stage fluorescence microscope (DM LFS) with EL 6000 light source was placed on a portable platform with an active vibration insulation table (AVI-200/LP, Herzan), and the Sutter Instruments micromanipulator model MPC-200 was put on a stable platform on the scaffolding. We mounted individual source leaves on the fixed stage of the microscope, a drop of water was placed on the epidermis and a HCX Plan Apo ×63 lens that was not corrected for cover slips was immersed into the water for observation. Pico gauges were impaled into individual palisade parenchyma cells through the epidermis, and movies were recorded to document the compression of the pico gauge filling oil. Measurements were made in the morning (typically between 9:00 and 11:00) on actively transpiring and photosynthesizing branches. We calculated pressure as described previously[33], and measured turgor pressure in six leaves.

Data and image analysis. Image J (National Institutes of Health, Bethesda, MD, USA) was used for all image analyses. We calculated the lumen resistance for sieve tubes using Darcy's law (or Hagen–Poiseuille's law) as described in Results and estimated the plate resistance according to a previous study[28]. Although this model assumes that there is no radial transport, we acknowledge that sieve tubes are permeable along their length[65] and radial permeability can influence how flow speed scales with tube radius. However, previous work indicates that viscous effects are dominant in transport phloem[66,67], therefore justifying our use of this model. It is also important to note that >50% of the viscous resistance comes from sieve plates, which will be unaffected by radial permeability.

In the phloem, resistance per length was calculated by adding the average plate and lumen resistance and dividing the number by the average sieve element length. In the xylem, we estimated the vessel lumen resistance per length and doubled it to estimate the resistance per length for an entire vessel, as previous research shows that lumen resistance and endwall resistance in the xylem are equal[45].

We used anatomical data collected from the top samples of each tree to test how influential pore number was to plate resistance in the data set. We calculated the plate resistance of the original data from the top of the trees and then increased the pore number by 130 for each tree. We then compared these estimates with the original data to determine how much resistance had increased by altering this parameter and checked that this increase would not cause the covering fraction of the plate to be greater than one.

Statistical analysis. Data normality was tested using the Shapiro–Wilk test, and unless specified, the data were log-transformed to fix non-normality. Variation within individual trees was examined using ANOVA and the Tukey honest significance difference test, and samples from the top and bottom of plants were compared using a two-sided, paired *t*-test. LR was used to compare different anatomical parameters and to test the relationship between these parameters and height. The only parameter for which log transformation did not correct normality was the number of sieve areas per plate. For analysing within plant variation in this trait, we used the Kruskal–Wallis non-parametric test. All statistical analyses were completed in JMP Pro 13.

Life Sciences Reporting Summary. Further information on experimental design is available in the Life Sciences Reporting Summary.

Data availability. The data that support the findings of this study are available from the corresponding author upon request.

Received: 26 June 2017; Accepted: 27 October 2017;
Published online: 4 December 2017

References

1. Knoblauch, M. & Oparka, K. The structure of the phloem—still more questions than answers. *Plant J.* **70**, 147–156 (2012).
2. De Schepper, V., De Swaef, T., Bauweraerts, I. & Steppe, K. Phloem transport: a review of mechanisms and controls. *J. Exp. Bot.* **64**, 4839–4850 (2013).
3. Münch, E. *Material Flow in Plants* (trans. Milburn, J. A. & Kreeb, K. H., Univ. Bremen, 2003) (Gustav Fischer, Jena, 1930).
4. Thompson, M. V. & Holbrook, N. M. Scaling phloem transport: water potential equilibrium and osmoregulatory flow. *Plant Cell Environ.* **26**, 1561–1577 (2003).
5. Jensen, K. H., Rio, E., Hansen, R., Clanet, C. & Bohr, T. Osmotically driven pipe flows and their relation to sugar transport in plants. *J. Fluid Mech.* **636**, 371–396 (2009).
6. LaBarbera, M. Principles of design of fluid transport systems in zoology. *Science* **249**, 992–1000 (1990).
7. Knoblauch, M. et al. Testing the Münch hypothesis of long distance phloem transport in plants. *eLife* **5**, e15341 (2016).
8. Lalonde, S., Wipf, D. & Frommer, W. B. Transport mechanisms for organic forms of carbon and nitrogen between source and sink. *Annu. Rev. Plant Biol.* **55**, 341–372 (2004).
9. Rennie, E. A. & Turgeon, R. A comprehensive picture of phloem loading strategies. *Proc. Natl Acad. Sci. USA* **106**, 14162–14167 (2009).
10. Turgeon, R. The puzzle of phloem pressure. *Plant Physiol.* **154**, 578–581 (2010).
11. West, G. B., Brown, J. H. & Enquist, B. J. A general model for the structure and allometry of plant vascular systems. *Nature* **400**, 664–667 (1999).
12. McCulloh, K. A., Sperry, J. S. & Adler, F. R. Water transport in plants obeys Murray's law. *Nature* **421**, 939–942 (2003).
13. Murray, C. D. The physiological principle of minimum work: I. The vascular system and the cost of blood volume. *Proc. Natl Acad. Sci. USA* **12**, 207–214 (1926).
14. Anfodillo, T., Carraro, V., Carrer, M., Fior, C. & Rossi, S. Convergent tapering of xylem conduits in different woody species. *New Phytol.* **169**, 279–290 (2006).

15. Mencuccini, M. Hydraulic constraints in the functional scaling of trees. *Tree Physiol.* **22**, 553–565 (2002).
16. Enquist, B. J. Cope's rule and the evolution of long-distance transport in vascular plants: allometric scaling, biomass partitioning and optimization. *Plant Cell Environ.* **26**, 151–161 (2003).
17. Savage, V. M. et al. Hydraulic trade-offs and space filling enable better predictions of vascular structure and function in plants. *Proc. Natl Acad. Sci. USA* **107**, 22722–22727 (2010).
18. Turgeon, R. & Wolf, S. Phloem transport: cellular pathways and molecular trafficking. *Annu. Rev. Plant Biol.* **60**, 207–221 (2009).
19. van Bel, A. J. E., Ehlers, K. & Knoblauch, M. Sieve elements caught in the act. *Trends Plant Sci.* **7**, 126–132 (2002).
20. Eschrich, W. in *Transport in Plants I: Phloem Transport (Encyclopedia of Plant Physiology)* Vol. 1 (eds Zimmermann, M. H. & Milburn, J. A.) 39–56 (Springer, Berlin, 1975).
21. Jensen, K. H. et al. Optimality of the Münch mechanism for translocation of sugars in plants. *J. R. Soc. Interface* **8**, 1155–1165 (2011).
22. Pickard, W. F. Münch without tears: a steady-state Münch-like model of phloem so simplified that it requires only algebra to predict the speed of translocation. *Funt. Plant Biol.* **39**, 531–537 (2012).
23. Hölttä, T., Mencuccini, M. & Nikinmaa, E. Linking phloem function to structure: analysis with a coupled xylem–phloem transport model. *J. Theor. Biol.* **259**, 325–337 (2009).
24. Petit, G. & Crivellaro, A. Comparative axial widening of phloem and xylem conduits in small woody plants. *Trees* **28**, 915–921 (2014).
25. Jyske, T. & Hölttä, T. Comparison of phloem and xylem hydraulic architecture in *Picea abies* stems. *New Phytol.* **205**, 102–115 (2015).
26. Rosner, S., Baier, P. & Kikuta, S. B. Osmotic potential of Norway spruce *Picea abies* (L.) Karst. secondary phloem in relation to anatomy. *Trees* **15**, 472–482 (2001).
27. Woodruff, D. R. The impacts of water stress on phloem transport in Douglas-fir trees. *Tree Physiol.* **34**, 5–14 (2014).
28. Jensen, K. H. et al. Modeling the hydrodynamics of phloem sieve plates. *Front. Plant Sci.* **3**, 151 (2012).
29. Liesche, J., Pace, M. R., Xu, Q., Li, Y. & Chen, S. Height-related scaling of phloem anatomy and the evolution of sieve element end wall types in woody plants. *New Phytol.* **214**, 245–256 (2017).
30. Knoblauch, M. & Peters, W. S. What actually is the Münch hypothesis? A short history of assimilate transport by mass flow. *J. Integr. Plant Biol.* **59**, 292–310 (2017).
31. Ryan, M. G. & Asao, S. Phloem transport in trees. *Tree Physiol.* **34**, 1–4 (2014).
32. Mullendore, D. L., Windt, C. W., Van As, H. & Knoblauch, M. Sieve tube geometry in relation to phloem flow. *Plant Cell* **22**, 579–593 (2010).
33. Knoblauch, J., Mullendore, D. L., Jensen, K. H. & Knoblauch, M. Pico gauges for minimally invasive intracellular hydrostatic pressure measurements. *Plant Physiol.* **166**, 1271–1279 (2014).
34. Jensen, K. H., Savage, J. A. & Holbrook, N. M. Optimal concentration for sugar transport in plants. *J. R. Soc. Interface* **10**, 20130055 (2013).
35. Liesche, J., Windt, C., Bohr, T., Schulz, A. & Jensen, K. H. Slower phloem transport in gymnosperm trees can be attributed to higher sieve element resistance. *Tree Physiol.* **35**, 376–386 (2015).
36. De Schepper, V. et al. ^{11}C-PET imaging reveals transport dynamics and sectorial plasticity of oak phloem after girdling. *Front. Plant Sci.* **4**, 200 (2013).
37. Canny, M. J. *Phloem Translocation* 205–207 (Cambridge Univ. Press, Cambridge, 1973).
38. Windt, C. W., Vergeldt, F. J., De Jager, P. A. & Van As, H. MRI of long-distance water transport: a comparison of the phloem and xylem flow characteristics and dynamics in poplar, castor bean, tomato and tobacco. *Plant Cell Environ.* **29**, 1715–1729 (2006).
39. Gould, N., Thorpe, M. R., Koroleva, O. & Minchin, P. E. H. Phloem hydrostatic pressure relates to solute loading rate: a direct test of the Münch hypothesis. *Funt. Plant Biol.* **32**, 1019–1026 (2005).
40. Oner-Sieben, S. & Lohaus, G. Apoplastic and symplastic phloem loading in *Quercus robur* and *Fraxinus excelsior*. *J. Exp. Bot.* **65**, 1905–1916 (2014).
41. Liesche, J., Martens, H. J. & Schulz, A. Symplasmic transport and phloem loading in gymnosperm leaves. *Protoplasma* **248**, 181–190 (2011).
42. Croser, C., Bengough, A. G. & Pritchard, J. The effect of mechanical impedance on root growth in pea (*Pisum sativum*). II. Cell expansion and wall rheology during recovery. *Physiol. Plant.* **109**, 150–159 (2000).
43. Pritchard, J. Aphid stylectomy reveals an osmotic step between sieve tube and cortical cells in barley roots. *J. Exp. Bot.* **47**, 1519–1524 (1996).
44. Rygol, J., Pritchard, J., Zhu, J. J., Tomos, A. D. & Zimmermann, U. Transpiration induces radial turgor pressure gradients in wheat and maize roots. *Plant Physiol.* **103**, 493–500 (1993).
45. Sperry, J. S., Hacke, U. G. & Wheeler, J. K. Comparative analysis of end wall resistivity in xylem conduits. *Plant Cell Environ.* **28**, 456–465 (2005).
46. van Bel, A. J. E. The phloem, a miracle of ingenuity. *Plant Cell Environ.* **26**, 125–149 (2003).
47. Fensom, D. S. The bio-electric potentials of plants and their functional signficance: I. An electrokinetic theory of transport. *Can. J. Bot.* **35**, 573–582 (1957).
48. Spanner, D. C. The translocation of sugar in sieve tubes. *J. Exp. Bot.* **9**, 332–342 (1958).
49. Lang, A. Relay mechanism for phloem translocation. *Ann. Bot.* **44**, 141–145 (1979).
50. Aikman, D. P. Contractile proteins and hypotheses concerning their role in phloem transport. *Can. J. Bot.* **58**, 826–832 (1980).
51. Comtet, J., Jensen, K. H., Turgeon, R., Stroock, A. D. & Hosoi, A. E. Passive phloem loading and long-distance transport in a synthetic tree-on-a-chip. *Nat. Plants* **3**, 17032 (2017).
52. Turgeon, R., Medville, R. & Nixon, K. C. The evolution of minor vein phloem and phloem loading. *Am. J. Bot.* **88**, 1331–1339 (2001).
53. Gamalei, Y. Phloem loading and its development related to plant evolution from trees to herbs. *Trees* **5**, 50–64 (1991).
54. Carvalho, M. R., Turgeon, R., Owens, T. & Niklas, K. J. The scaling of the hydraulic architecture in poplar leaves. *New Phytol.* **214**, 145–157 (2017).
55. Woodruff, D. R., Bond, B. J. & Meinzer, F. C. Does turgor limit growth in tall trees? *Plant Cell Environ.* **27**, 229–236 (2004).
56. Ryan, M. G. & Yoder, B. J. Hydraulic limits to tree height and tree growth. *Bioscience* **47**, 235–242 (1997).
57. Koch, G. W., Sillett, S. C., Jennings, G. M. & Davis, S. D. The limits to tree height. *Nature* **428**, 851–854 (2004).
58. Mencuccini, M., Hölttä, T. & Martínez-Vilalta, J. in *Size- and Age-Related Changes in Tree Structure and Function* (eds Meinzer, F. C. et al.) 309–339 (Springer, New York, NY, 2011).
59. Aloni, R. Control of xylogenesis within the whole tree. *Ann. For. Sci.* **46**, 267s–272s (1989).
60. Anfodillo, T. et al. Widening of xylem conduits in a conifer tree depends on the longer time of cell expansion downwards along the stem. *J. Exp. Bot.* **63**, 837–845 (2012).
61. Savage, J. A., Haines, D. F. & Holbrook, N. M. The making of giant pumpkins: how selective breeding changed the phloem of *Cucurbita maxima* from source to sink. *Plant Cell Environ.* **38**, 1543–1554 (2015).
62. Savage, J. A. et al. Allocation, stress tolerance and carbon transport in plants: how does phloem physiology affect plant ecology? *Plant Cell Environ.* **39**, 709–725 (2016).
63. Scholz, A., Klepsch, M., Karimi, Z. & Jansen, S. How to quantify conduits in wood? *Front. Plant Sci.* **4**, 56 (2013).
64. Ruzin, S. E. *Plant Microtechnique and Microscopy* 132 (Oxford Univ. Press, Oxford, 1999).
65. Phillips, R. J. & Dungan, S. R. Asymptotic analysis of flow in sieve tubes with semi-permeable walls. *J. Theor. Biol.* **162**, 465–485 (1993).
66. Thompson, M. V. & Holbrook, N. M. Application of a single-solute non-steady-state phloem model to the study of long-distance assimilate transport. *J. Theor. Biol.* **220**, 419–455 (2003).
67. Jensen, K. H. et al. Sap flow and sugar transport in plants. *Rev. Mod. Phys.* **88**, 035007 (2016).

Acknowledgements

Funding was provided by the National Science Foundation (IOS 1021779 and 1456682 to N.M.H. and M.K.), a Katharine H. Putnam Fellowship in Plant Science (J.A.S.), a Harvard Bullard Fellowship (M.K.), and the University of Minnesota Duluth (J.A.S.). Samples were collected at the Arnold Arboretum of Harvard University (permit no. 22-2013), the Harvard Forest and the main campus of Harvard University. Imaging was completed at the Harvard Center for Biological Imaging, Franceschi Microscopy and Imaging Center at WSU, the Center for Nanoscale Systems (Harvard University) and the Weld Hill Microscopy Lab at the Arnold Arboretum.

Author contributions

J.A.S., K.H.J., M.K. and N.M.H. designed the research. J.A.S., S.D.B., L.C., J.T.G., J.K., M.K. and J.M.L. collected the data and standardized protocols. J.A.S. and K.H.J. analysed the data. J.A.S., N.M.H., K.H.J. and M.K. wrote the paper.

Competing interests

The authors declare no competing financial interests.

Additional information

Supplementary information is available for this paper at https://doi.org/10.1038/s41477-017-0064-y.

Reprints and permissions information is available at www.nature.com/reprints.

Correspondence and requests for materials should be addressed to J.A.S.

Publisher's note: Springer Nature remains neutral with regard to jurisdictional claims in published maps and institutional affiliations.

nature research

Corresponding author(s): Savage, Jessica

☐ Initial submission ☐ Revised version ☒ Final submission

Life Sciences Reporting Summary

Nature Research wishes to improve the reproducibility of the work that we publish. This form is intended for publication with all accepted life science papers and provides structure for consistency and transparency in reporting. Every life science submission will use this form; some list items might not apply to an individual manuscript, but all fields must be completed for clarity.

For further information on the points included in this form, see Reporting Life Sciences Research. For further information on Nature Research policies, including our data availability policy, see Authors & Referees and the Editorial Policy Checklist.

Experimental design

1. Sample size

Describe how sample size was determined.

We replicated xylem anatomical measurements based on established standards and we chose a replication of the phloem anatomical parameters that had a similar coefficient of variation to the xylem data.

2. Data exclusions

Describe any data exclusions.

No exclusions.

3. Replication

Describe whether the experimental findings were reliably reproduced.

All attempts at replication were successful.

4. Randomization

Describe how samples/organisms/participants were allocated into experimental groups.

This is not relevant to this study because all samples were treated the same.

5. Blinding

Describe whether the investigators were blinded to group allocation during data collection and/or analysis.

Samples were assigned a unique number but blinding in this type of study is not possible because the anatomy samples are easily identifiable to the species-level.

Note: all studies involving animals and/or human research participants must disclose whether blinding and randomization were used.

6. Statistical parameters

For all figures and tables that use statistical methods, confirm that the following items are present in relevant figure legends (or in the Methods section if additional space is needed).

n/a	Confirmed	
☐	☒	The exact sample size (*n*) for each experimental group/condition, given as a discrete number and unit of measurement (animals, litters, cultures, etc.)
☐	☒	A description of how samples were collected, noting whether measurements were taken from distinct samples or whether the same sample was measured repeatedly
☒	☐	A statement indicating how many times each experiment was replicated
☐	☒	The statistical test(s) used and whether they are one- or two-sided (note: only common tests should be described solely by name; more complex techniques should be described in the Methods section)
☒	☐	A description of any assumptions or corrections, such as an adjustment for multiple comparisons
☐	☒	The test results (e.g. *P* values) given as exact values whenever possible and with confidence intervals noted
☐	☒	A clear description of statistics including central tendency (e.g. median, mean) and variation (e.g. standard deviation, interquartile range)
☐	☒	Clearly defined error bars

See the web collection on statistics for biologists for further resources and guidance.

Software

Policy information about availability of computer code

7. Software

Describe the software used to analyze the data in this study.	JMP Pro 13 and ImageJ

For manuscripts utilizing custom algorithms or software that are central to the paper but not yet described in the published literature, software must be made available to editors and reviewers upon request. We strongly encourage code deposition in a community repository (e.g. GitHub). *Nature Methods* guidance for providing algorithms and software for publication provides further information on this topic.

Materials and reagents

Policy information about availability of materials

8. Materials availability

Indicate whether there are restrictions on availability of unique materials or if these materials are only available for distribution by a for-profit company.	No unique materials used.

9. Antibodies

Describe the antibodies used and how they were validated for use in the system under study (i.e. assay and species).	No antibodies used.

10. Eukaryotic cell lines

a. State the source of each eukaryotic cell line used.	No cell lines used.
b. Describe the method of cell line authentication used.	No cell lines used.
c. Report whether the cell lines were tested for mycoplasma contamination.	No cell lines used.
d. If any of the cell lines used are listed in the database of commonly misidentified cell lines maintained by ICLAC, provide a scientific rationale for their use.	No cell lines used.

Animals and human research participants

Policy information about studies involving animals; when reporting animal research, follow the ARRIVE guidelines

11. Description of research animals

Provide details on animals and/or animal-derived materials used in the study.	No animals were used.

Policy information about studies involving human research participants

12. Description of human research participants

Describe the covariate-relevant population characteristics of the human research participants.	No human research participants.